Clim. Past Discuss., 8, 5787–5816, 2012
www.clim-past-discuss.net/8/5787/2012/
doi:10.5194/cpd-8-5787-2012

Climate of the Past Discussions

Influence of dynamic vegetation on climate change and terrestrial carbon storage in the Last Glacial Maximum

R. O'ishi[1,2] **and A. Abe-Ouchi**[1,3]

[1]Atmosphere and Ocean Research Institute, University of Tokyo, Kashiwa, Japan
[2]National Institute of Polar Research, Tokyo, Japan
[3]Frontier Research Center for Global Change, Yokohama, Japan

Received: 5 November 2012 – Accepted: 12 November 2012 – Published: 27 November 2012

Correspondence to: R. O'ishi (ryo@aori.u-tokyo.ac.jp)

Published by Copernicus Publications on behalf of the European Geosciences Union.

Abstract

When the climate is reconstructed from paleoevidence, it shows that the Last Glacial Maximum (LGM, ca. 21 000 yr ago) is cold and dry compared to the present day. Reconstruction also shows that compared to today, the vegetation of the LGM is less active and the distribution of vegetation was drastically different, due to cold temperature, dryness, and a lower level of atmospheric CO_2 level (185 ppm compared to a preindustrial level of 285 ppm). In the present paper, we investigate the influence of vegetation change on the climate of the LGM by using a coupled atmosphere-ocean-vegetation general circulation model (GCM, the MIROC-LPJ). We examined four GCM experiments (LGM and preindustrial, with and without vegetation feedback) and quantified the strength of the vegetation feedback during the LGM. The result shows global-averaged cooling during the LGM is amplified by +13.5 % due to the introduction of vegetation feedback. This is mainly caused by the increase of land surface albedo due to the expansion of tundra in northern high latitudes and the desertification in northern middle latitudes around 30° N to 60° N. We also investigated how this change in climate affected the total terrestrial carbon storage by using a separated Lund-Potsdam-Jena dynamic global vegetation model (LPJ-DGVM). Our result shows that the total terrestrial carbon storage was reduced by 653 PgC during the LGM, which corresponds to the emission of 308 ppm atmospheric CO_2. The carbon distribution during the LGM that is predicted from using an atmospheric-ocean-vegetation (AOV) GCM and using the LPJ-DGVM after an atmospheric-ocean (AO) GCM, is generally the same, but the difference is not negligible for explaining the lowering of atmospheric CO_2 during the LGM.

1 Introduction

Paleoenvironmental reconstructions indicate a cold period around 21 000 yr ago, known as the Last Glacial Maximum (LGM), which is characterized by the huge

CPD
8, 5787–5816, 2012

extension of an ice sheet and lower atmospheric CO_2 concentration. Reconstruction indicates that two huge ice sheets covered the northern part of the North American continent and northern Europe (Peltier, 1994, 2004). An equivalent amount of sea water is reduced from the LGM ocean, so that sea level during the LGM is lower by 120 to 150 m than that of the present day (Yokoyama et al., 2000). Paleo-ocean reconstruction shows about 2 to 3 °C cooling of the sea-surface temperature compared to the present day in the tropical ocean and more than 10 °C cooling in high latitudes (CLIMAP Project Members, 1976, 1984; Kucera et al., 2005). Pollen-based reconstruction also indicates more than 10 °C cooling of ice-free land in North America and Europe (Bartlein et al., 2011). A cooler climate reduces precipitation, thus the land surface is drier than it is in the present day (Kohfeld and Harrison, 2000; Yu et al.). Reconstructed information from ice-core components indicates that the atmospheric CO_2 concentration during the LGM is about 185 ppm (Jouzel et al., 1993; Monnin et al., 2001), which is 100 ppm lower than it is in preindustrial times (285 ppm). Due to these cool, dry, and low-CO_2 conditions, the vegetation distribution during the LGM is different from that of today in that it included an expanded arid area, a southward shift of the boreal forest belt, and a southward expansion of tundra (Prentice and Webb, 1998; Prentice and Jolly, 2000; Prentice and Harrison, 2009).

The paleoclimate modeling community tried to reproduce the LGM climate by using atmosphere general circulation models (AGCMs) and coupled atmosphere-ocean general circulation models (AOGCMs) in the Paleoclimate Modeling Intercomparison Project (PMIP). The results of the PMIP show that general circulation models (GCMs) are generally able to reproduce consistent cooling (Joussaume and Taylor, 2000; Braconnot et al., 2007). The paleovegetation distribution during the LGM is also investigated, using a vegetation models that use GCM results as input. This predicted qualitatively consistent vegetation changes (Harrison and Prentice, 2003; Prentice et al., 2011). The latest GCMs have been developed as coupled atmosphere-ocean-vegetation GCMs (AOVGCMs), which predict consistent vegetation change within individual coupled GCM experiments. By using this kind of GCM, these models generally

CPD
8, 5787–5816, 2012

predict the same tendencies of vegetation change during the LGM as compared to the present day (Wyputta and McAvaney, 2001; Crucifix et al., 2005a,b; Crucifix and Hewitt, 2005; Jahn et al., 2005; Henrot et al., 2009). These results reveal how changes in the land surface during the LGM contributes to the climate through changes of surface heat and water balance. Dust emission change due to vegetation change is also noted as an important factor of the vegetation during the LGM (Mahowald et al., 2006; Takemura et al., 2009).

Another aspect of vegetation change during the LGM is the change in the carbon cycle that affects atmospheric CO_2 concentration. Not only the distribution of vegetation but also the strength of photosynthesis is an important factor in terrestrial carbon distribution (Gerber et al., 2004; Prentice and Harrison, 2009). As far as the terrestrial carbon storage, reconstruction indicates a 300 to 700 PgC reduction during the LGM (Bird et al., 1994), and estimation by GCM LGM simulation models shows almost the same range of terrestrial carbon reduction (Prentice et al., 1993; Friedlingstein et al., 1995; François et al., 1998, 1999; Kaplan et al., 2002; Otto et al., 2002; Köhler and Fischer, 2004; Köhler et al., 2005; Ciais et al., 2011). The uncertainty around the amount of terrestrial carbon stored during the LGM is thus larger than 200 PgC, which is equivalent to a reduction in the atmosphere of 100 ppm CO_2 (Jouzel et al., 1993; Monnin et al., 2001). If we consider the sea-level change during the LGM, about 200 PgC of terrestrial carbon could have been stored in the exposed continental shelf (Faure et al., 1996; Zeng, 2003; Montenegro et al., 2006), and the uncertainty in this may be comparable to that of the change in atmospheric CO_2.

As shown above, there is uncertainty in the amount of change in terrestrial carbon, but it is important for understanding the LGM environment, especially the change in atmospheric CO_2. In the present study, we apply an AOVGCM so that we could assume that there is vegetation feedback to the climate and the resultant equilibrium carbon storage during the LGM. In order to save integration time, we use the resultant equilibrium climate of this LGM AOVGCM as input to a separated vegetation module of an AOVGCM, but the equilibrium carbon storage is equivalent to that from the AOVGCM

CPD
8, 5787–5816, 2012

after integrating for a very long time. In the present study, we separate terrestrial carbon storage into three kinds: response to the LGM climate, washout by ice-sheet coverage, and the stock on the exposed continental shelf. We also apply the AOGCM for the LGM in order to evaluate the vegetation-climate feedback during the LGM and to use the equilibrium climate as input to the vegetation module, and also to estimate how vegetation evaluation after the AOGCM differs from the result that was consistent with those of the AOVGCM.

2 Model description

2.1 Model components

In the present study, a coupled vegetation general circulation model MIROC-LPJ (O'ishi and Abe-Ouchi, 2009) is used with a bias-correction procedure (O'ishi and Abe-Ouchi, 2011) in order to remove the GCM bias and to predict the correct distribution of vegetation and consistent response to the paleoclimate. The atmosphere component of the MIROC-LPJ is CCSR/NIES/FRCGC AGCM (Center for Climate System Research/National Institute for Environmental Studies/Frontier Research Center for Global Change atmospheric general circulation model), which is part of an atmosphere-ocean general circulation model (AOGCM) (Hasumi and Emori, 2004) that contributed to IPCC AR4 (Meehl et al., 2007). The dynamical vegetation component is the Lund-Potsdam-Jena Dynamic Global Vegetation Model (LPJ-DGVM) (Sitch et al., 2003), which predicts the distribution of ten vegetation types (plant functional types, PFTs) based on the bioclimatic limits, photosynthesis, respiration, carbon allocation, plant establishment, growth, turnover, mortality, and competition among the PFTs. In the MIROC-LPJ, an interactive coupling between the atmosphere and the change in land vegetation is introduced as follows: the monthly mean surface temperature, precipitation, and cloud cover predicted by the AGCM are used as the input to the LPJ-DGVM. The distribution of the PFTs predicted by the LPJ-DGVM are translated into

CPD
8, 5787–5816, 2012

ten vegetation types, which are assumed in MATSIRO (Takata et al., 2003), the MIROC land-surface scheme, taken from a modified conversion table from BIOME3 (Haxeltine and Prentice, 1996; O'ishi and Abe-Ouchi, 2009). The land surface parameters are changed annually in MATSIRO, along with the vegetation change predicted by the LPJ-DGVM. In all the experiments, the horizontal and vertical resolutions of the atmospheric grid points correspond to T42 ($2.8 \times 2.8^{\circ}$) and 20 layers, respectively. The ocean component is a slab-ocean that assumes a seasonal transport of ocean heat.

2.2 Bias correction

The MIROC generally reproduces the climate of today and the 20th century, but there is an unavoidable problem of temperature and precipitation bias in the MIROC. This bias can cause an incorrect distribution of vegetation in the control and present day, and thus can cause a false response of the atmosphere to the change of vegetation distribution in the paleo-setting experiments. Hence we introduce a bias correction into the MIROC-LPJ. The temperature and precipitation from the AGCM are modified by using a reference model experiment and observed data, in order to remove the bias before these variables are passed to the LPJ-DGVM. We choose the ECMWF ERA40 data (Uppala et al., 2005) and the CPC Merged Analysis of Precipitation (Xie and Arkin, 1997) for the observed temperature and precipitation, respectively. Detailed formulation is described in O'ishi and Abe-Ouchi (2011).

2.3 Carbon balance

The LPJ-DGVM is able to predict four types of vegetation carbon storage (leaf, heartwood, sapwood, and root) for every PFT, and three soil-based carbon pools that correspond to different timescales of decomposition, in a coupled MIROC-LPJ. However, feedback through carbon balance is not introduce in the MIROC-LPJ, and both the MIROC and LPJ-DGVM are forced by a given level of atmospheric CO_2, because the MIROC-LPJ lacks an ocean carbon module. Prediction of the equilibrium terrestrial

CPD
8, 5787–5816, 2012

carbon is done by a separated LPJ-DGVM experiment using as input the result of the MIROC-LPJ equilibrium climate. This is done because it takes many integrations to equilibrate the terrestrial carbon storage by a coupled MIROC-LPJ (see Experimental settings, below).

3 Experimental settings

3.1 Coupled GCM experiments

Two experiments are preformed by using the MIROC-LPJ, as shown in Table 1. In the CTL experiment, AOV (PI), the preindustrial level of atmospheric CO_2 (285 ppm) and present-day orbital elements are employed. In the LGM experiment, AOV (LGM), the LGM level of atmospheric CO_2(185 ppm), the LGM orbital elements, the expanded LGM land cover ($+23 \times 10^{12}$ m^2 which is equivalent to a 150 m sea-level descent), and ice sheets (Peltier, 2004) are employed. These experiments are integrated over about 400 yr including spin-up, which is enough long to reach equilibrium for both vegetation distribution and climate. An additional set of experiments, AO (PI) and AO (LGM), are performed to investigate the effect of vegetation change upon climate. In these experiments, the model do not contain the LPJ-DGVM, and the vegetation map is fixed to the equilibrium state of the AOV (PI) experiment. Since land cover during the LGM is extended compared to that of the present day, in order to prepare a vegetation map in the AO (LGM), a separated LPJ-DGVM experiment is performed using the LGM land cover with the AOV (PI) result as input. This map is the same as the resultant vegetation map of the AOV (PI) for those land grids that are shared by both the CTL and the LGM. Results of the last 50 yr in all experiments are used for the analysis because vegetation distribution is sufficiently equilibrated after two AOV experiments.

CPD
8, 5787–5816, 2012

3.2 Separated LPJ-DGVM experiments

3.2.1 Sensitivity experiments

We perform three sensitivity experiments, as shown in Table 2, in order to compare the impact of CO_2 concentration, precipitation, and temperature on vegetation distribution during the LGM. These experiments lack one of the LGM environments (CO_2, precipitation, and temperature), and those of the preindustrial era are used instead of the LGM values. For example, experiment CP do not include the effect of the LGM temperature, so we can evaluate the impact of the temperature change during the LGM by comparing this with the result of the AOV (LGM).

3.2.2 Carbon equilibrium

Since changes in soil carbon have a long timescale, four hundred years are too short to equilibrate the total terrestrial carbon storage. In order to evaluate the equilibrium carbon storage in the LGM and the preindustrial era, separate LPJ-DGVM experiments are performed, using the result of the last 50 yr in the two AOV GCM experiments as input and letting them run for the equivalent of 1000 yr. The vegetation map and the climate are equilibrated far faster then is terrestrial carbon storage, so this us done so that it us not necessary to integrate a coupled MIROC-LPJ until carbon storage is equilibrated. This is the same procedure as was adopted in a previous study (O'ishi and Abe-Ouchi, 2009). We also examine separated LPJ-DGVM experiments, using the result of the AO (LGM) experiment as input. This experiment corresponds to the traditional offline diagnosis of carbon storage using a GCM result without vegetation change.

CPD
8, 5787–5816, 2012

4 Results

4.1 LGM climate and impact of vegetation change

In the AOV (LGM), the globally averaged surface air temperature is decreased by 4.88 K compared to the AOV (PI), due to orbital change, lowered atmospheric CO_2, expansion of the ice sheets, and changes in vegetation. On the other hand, in the AO (LGM), globally averaged surface air temperature is decreased by 4.29 K compared to the AO (PI). Thus change of vegetation contributes −0.58 K to global cooling, which corresponds to 13.5 % amplification of global cooling compared AO results. The distribution of temperature change in the AOV (LGM) (Fig. 1a) shows a strong cooling over the ice sheets in North America and northern Europe. In other land areas in the Northern Hemisphere, cooling is around 4 K to 8 K. Cooling due to vegetation change is mainly located around the middle latitudes of the Northern Hemisphere (Fig. 1b). In this area, a change of vegetation from forest to tundra or desert increase the land surface albedo (Fig. 1c). In Eurasia, more than 30 % (at most 80 %) of the total cooling at around 45° N is due to vegetation change. In North America, except for the ice sheet, a contribution of vegetation change to the total cooling around 45° N exists, however, it is less than 30 %. Change of vegetation contributes to the cooling not only over land but also on the ocean. Around 45° N, a southern shift of the sea-ice boundary significantly increases the surface albedo (Fig. 1c) in south of Nova Scotia. A slight increase in albedo is seen in the northwestern part of the Pacific Ocean. In the tropical region, a slight warming occurs due to vegetation change. This is directly from the increase of sensible heat, which is caused by a reduction in evaporation and precipitation. During the LGM precipitation mainly decreased (Fig. 1d). A significant change is seen in the tropical rain belt and the middle- to high-latitude continental areas in the Northern Hemisphere. The precipitation-change ratio shows a more than 60 % reduction in precipitation in central Eurasia, the African Sahel, and Hudson Bay (Fig. 1e). The ratio of precipitation change due to vegetation change to the precipitation of the CTL is most significant in the African Sahel (Fig. 1f).

CPD
8, 5787–5816, 2012

4.2 Vegetation distribution

In the AOV (LGM), there are some typical changes in the vegetation pattern compared to the AOV (PI) (Fig. 2a and b). In the south of the Scandinavian and Laurentide ice sheets, boreal forests shift southward and tundra appears. In eastern Siberia, boreal forests retreat southward and the southern boundary of tundra is relocated to 50° N. The southern boundary of the boreal forests also shifts southward in North America and China. In the downstream region of the Scandinavian ice sheet, a slight northward shift of boreal forest appears. Total reduction of the area of boreal forest is $14.0 \times 10^{12}\,m^2$ and expansion of tundra is $6.2 \times 10^{12}\,m^2$. Expansion of desert is seen in Central Asia, North and South Africa, and North America, totaling $15.1 \times 10^{12}\,m^2$. In the tropical region, the tropical forest shrinks, and savanna or grassland appears or increases, especially in Africa. Tropical forest covers the exposed continental shelf over the maritime continent. The continental shelf of the East China Sea to south of the Japan Sea is covered by temperate forest. The East Siberian Sea and north of the Bering Sea turns into tundra. The net primary productivity (NPP) also shows a drastic change (Fig. 3a and b). The globally averaged annual NPP during the LGM and the PI are $59.4\,PgC\,yr^{-1}$ and $44.6\,PgC\,yr^{-1}$, respectively. Reduction of $5.4\,PgC\,yr^{-1}$ occurs due to covering by the expanded ice sheet, and an increase of $7.8\,PgC\,yr^{-1}$ occurs on the exposed continental shelf due to a change in sea level. In the PI experiment, a large part of the total reduction of NPP is seen in the forest region. By performing additional sensitivity experiments using a separated LPJ-DGVM, it is revealed that these vegetation changes are caused by individual aspects of environmental change during the LGM. Figure 2c and 2b show that the temperature changes during the LGM mainly dominated the distribution of forest. Cooling in high latitudes shifts the boundary of the tundra/forest to the south. Around the Scandinavian and Laurentide ice sheets, tundra appears between the ice sheet and the boreal forest, due to cooling. In the tropical regions, cooling compensated for expansion of the arid areas, which are due to less precipitation and lower

CPD
8, 5787–5816, 2012

CO_2 during the LGM but a relatively higher PI temperature. The NPP distribution is higher in tropical regions when the LGM temperature is applied (Fig. 3c and b).

By comparing Fig. 2d and 2b, we see that precipitation changes during the LGM mainly dominated the distribution of desert and savanna. In the central Eurasia continent, less precipitation during the LGM expands deserts, especially north and west of the Caspian Sea, which had the largest decrease in precipitation on the Eurasian continent. The Gobi and Taklamakan deserts expands slightly northward. The boreal forests of the Pamir plateau and Tian Shan Mountains turns into desert, due to the decrease in precipitation. The southern boundary of the boreal forest agrees with the vegetation distribution and the NPP (Fig. 3d and b).

By comparing Fig. 2e and b, we see that low CO_2 during the LGM mainly dominated the distribution of savanna in the tropical region. There is a slight expansion of desert due to less photosynthesis, but the NPP showed a substantial reduction due to the level of CO_2 (Fig. 3e and b). These results suggest that the major factors that dominated the distribution of vegetation during the LGM are temperature and precipitation. Temperature defines the tundra/forest boundary, and precipitation is dominant in determining the desert/forest boundary. The lower atmospheric CO_2 during the LGM only changes the vegetation in savanna, but it reduces the NPP, especially in tropical regions, even when the vegetation distribution is unchanged.

There are also nonlinear effects of these three variables. In Amazonia and Africa, temperate forest replaces tropical forest, so that the tropical region shrink toward the equator. However, this is not only due to cooling but also to precipitation and CO_2. The southward shift of the tundra/forest boundary in northeast China is not explained by a single variable. A nonlinear effect of temperature, precipitation, and CO_2 causes the total response of vegetation in these regions.

4.3 Terrestrial carbon storage during the LGM

In the present study, we examined three separated LPJ-DGVM experiments in order to obtain the equilibrium carbon storage. Two AOV experiments and one AO experiment

CPD
8, 5787–5816, 2012

were chosen (see Table 1). The results of the AOV experiments are consistent with the AOVGCM equilibrium. The AO (LGM) case is used to quantify the uncertainty between the different methods, because it corresponds to a terrestrial carbon evaluation after the AOGCM result without vegetation-atmosphere interaction. The preindustrial AOV experiment shows 1094.9 PgC global vegetation carbon and 1727.3 global soil carbon, so that the total global carbon storage is 2822.2 PgC (Table 3). The LGM AOV experiment shows 830.3 PgC vegetation carbon and 1340.6 PgC soil carbon, so that the total global carbon storage is 2170.9 PgC (Table 3). In other words, during the LGM, the total terrestrial carbon storage is reduced by 651.6 PgC compared to that of the preindustrial era. Reduction of 264.6 PgC out of 651.6 PgC is due to the change in vegetation carbon, and 386.7 PgC is due to the change in soil carbon. The total reduction of terrestrial carbon during the LGM is equivalent to 307.4 ppm CO_2 emission to the atmosphere. On the other hand, by using the LGM AO result, the reduction of carbon storage during the LGM is slightly larger than that of the AOV result (Table 3). Global vegetation carbon and global soil carbon are 825.7 PgC and 1313.9 PgC, respectively. Hence reduction of total global carbon storage is 682.6 PgC, equivalent to 322.0 ppm CO_2 emission to the atmosphere.

During the LGM there is no vegetation in the areas covered by the ice sheets. Assuming the flow of the ice sheet completely washes out the soil carbon, there is no carbon storage under or over the ice sheet in the two LGM experiments. In the PI experiment our results show that 109.7 PgC vegetation carbon out of 1094.9 PgC, and 364.2 PgC soil carbon out of 1727.3 PgC, are removed by the LGM ice sheets in North America and Scandinavia. On the other hand, the continental shelf is exposed because of a descent in the sea level, so that terrestrial carbon can be stored there during the LGM. In the AOV experiment, 158.7 PgC vegetation carbon and 179.8 PgC soil carbon newly appears on the exposed continental shelf. In the AO experiment, these values are 163.3 PgC and 193.3 PgC, respectively. All the values in the two LGM experiments in Table 3 include both a reduction due to the ice sheet and an increase due to the extended continental shelf. In order to extract the response of the terrestrial carbon

CPD
8, 5787–5816, 2012

pools to the LGM climate, we leave out the areas of the ice sheets and continental shelves and listed their values in parentheses in Table 3. In the AOV (LGM), a 314 PgC reduction of vegetation carbon and a 203 PgC reduction of soil carbon occur due to the LGM climate and CO_2 level. In the AO (LGM), reduction of vegetation and soil carbon pools are 323 PgC and 243 PgC, respectively. Generally, the contribution of the LGM climate and extension of the ice sheet and continental shelf to the total carbon change (652 PgC) are −517 PgC, −474 PgC, and +338 PgC, respectively, in the AOV (LGM). In the AO (LGM), they are −566 PgC, −474 PgC, and +356 PgC, for a total change of 683 PgC.

In areas that do not experience an ice sheet or shelf exposure, the distribution of terrestrial carbon shows substantial changes that reflect the changes in distribution of vegetation. In the AOV (LGM), the most significant decrease of vegetation carbon occurs in the Siberian forest belt (Fig. 4a and c). Other forest areas also show a decrease in vegetation carbon, but typically less than 5 kgC m^{-2}, which is consistent with the decrease of NPP. The largest decrease of soil carbon is seen in East Siberia and Central Eurasia (Fig. 4d and f), which corresponds to the replacement of boreal forest by tundra. In other regions, the soil carbon shows a slight change, less than ±10 kgC m^{-2}. In the AO (LGM), distribution of terrestrial carbon storage is generally similar to that of the AOV (LGM) in both vegetation and soil carbon pools (Fig. 4b and e). Differences in these two LGM experiments Northern Hemisphere continent (soil carbon). These differences reflect the changes in habitable zones (vegetation carbon) and cooling (soil carbon) due to vegetation-climate feedback.

5 Discussion

5.1 Vegetation change and amplification of cooling

In the present study, our results indicate a cooler and drier climate than is shown in previous studies (Braconnot et al., 2007; Crucifix and Hewitt, 2005; Henrot et al., 2009).

CPD
8, 5787–5816, 2012

Compared to the latest reconstruction (Bartlein et al., 2011), cooling during the LGM is overestimated in both North America and Europe. On the other hand, cooling is underestimated in southern Africa. The pattern of precipitation change is generally the same as the reconstruction in North America and Europe, but the intensity of change is underestimated. We also obtained similar vegetation changes, such as expansion of tundra, a southward shift of boreal forests, and expansion of desert/arid regions, compared to previous studies (Prentice and Jolly, 2000; Harrison and Prentice, 2003; Crucifix et al., 2005b; Jahn et al., 2005; Henrot et al., 2009; Prentice et al., 2011). The resultant vegetation-climate feedback is positive, which has been shown in previous sensitivity studies (Crucifix et al., 2005a; Henrot et al., 2009). In the present study, the most dominant factor in the vegetation-climate model results is the increase in land surface albedo (Fig. 1c), which is due not only to the replacement of boreal forest by tundra and desert, but also to the increase in snow cover (not shown) in midlatitudes, in spite of the reduction in precipitation (Fig. 1f). In high latitudes, snow cover shows a slight decrease, and thus decreases the albedo, due to the reduction of precipitation that is caused by vegetation changes in the lower latitudes.

The MIROC-LPJ predicts a boreal forest band in western Siberia that is not seen in previous model studies using GCMs and vegetation models (Harrison and Prentice, 2003; Crucifix et al., 2005b; Prentice et al., 2011). In those studies, the boreal forest on the Eurasian continent is separated into east and west sections, or vanished completely. There are three possible explanations for this overestimation of boreal forest. First, the MIROC-LPJ shows a weaker cooling in western Siberia than do the PMIP2 model results (Braconnot et al., 2007). This weak cooling is not due to the positive vegetation-climate feedback in AOV (LGM), because the separated LPJ-DGVM run, using the result of the AO (LGM), predicts the same vegetation in this region (not shown). The second reason is related to the lack of fractional coverage representation in the land-surface scheme of the MIROC-LPJ. As described in O'ishi and Abe-Ouchi (2009), the land-surface scheme of the MIROC is able to handle only one vegetation type in a gridcell, and so it cannot handle fractional coverage. We defined the representations of

CPD
8, 5787–5816, 2012

the vegetation types by using variables from the coupled LPJ-DGVM; however, there can be an overestimation of a specific vegetation type, which is typically the most dominant vegetation type. In the LGM experiment in the present study, forest coverage in western Siberia was about 0.6, which was less than for the PI. However, this forest is assumed to occupy a whole gridcell in the land-surface scheme of the MIROC. Thus this treatment underestimates both the decrease in forest and the cooling due to vegetation feedback. If we could improve the MIROC-LPJfs fractional representation of the land-surface scheme, additional cooling by 1 to 2 °C would likely occur in western Siberia as well as in northeastern China and central Eurasia. On the other hand, the assumption of vegetation carbon storage shows a substantial decrease compared to the results of the PI (Fig. 4a and b).

5.2 Carbon storage

In the present study, the tendency of terrestrial carbon reduction of our results is similar to that of previous studies and falls into the typical range of uncertainty (Prentice et al., 1993; Friedlingstein et al., 1995; François et al., 1998, 1999; Kaplan et al., 2002; Otto et al., 2002; Köhler and Fischer, 2004) when using climate variables that include vegetation feedback. The total reduction of terrestrial carbon (−652 PgC) falls into the typical range of uncertainty (300 PgC to 700). We separated the total reduction of terrestrial carbon into three kinds: response to the LGM climate and CO_2, washout by ice-sheet coverage, and new stock on the exposed continental shelf.

Response of terrestrial biosphere to the cool, dry, and low-CO_2 LGM environment is seen in the reasonable reduction of the NPP (Fig. 3a and b), biomass (Fig. 4a and c), and vegetation coverage (Fig. 2a and b), as well as in previous studies. Soil carbon decreased during the LGM then the PI due to deactivation of photosynthesis, in spite of a lowering of the soil carbon decomposition speed (Lloyd and Taylor, 1994).

During the LGM, the assumption of washout by the ice sheet may overestimate the reduction of terrestrial carbon, because the carbon flux and storage in the present day that are predicted by the LPJ-DGVM tend to be larger than the typical values

CPD
8, 5787–5816, 2012

(Sitch et al., 2003; Denman et al., 2007) and those among multi-models (Cramer et al., 2001). The second reason is we do not know how much carbon was stored below an ice sheet during the LGM. We assumed all carbon is removed by the ice sheet, which has been assumed in previous studies. In this case, carbon washout depends on how much carbon was stored in the preindustrial control experiment. On the contrary, the Glacial Burial Hypothesis (Zeng, 2003, 2007) suggests that 500 PgC was buried under the LGM ice sheets. This value is comparable to −474 PgC, which we assumed to have been removed by the ice sheets. However, $\delta^{13}C$ reconstruction indicates that CO_2 rise during the last deglaciation is from ocean (Lourantou et al., 2010), which is consistent to our assumption of wash out.

Since we use a sea-level change of −150 m, which is the largest estimation (Yokoyama et al., 2000), the exposed ice-free continental shelf was maximized. In our model setting, the total area of exposed ice-free continental shelf is 23×10^{12} m^2, which is two times larger than that of previous studies (Zeng, 2003; Montenegro et al., 2006). If we apply a more moderate sea-level change, such as that noted in Montenegro et al. (2006), the increase of terrestrial carbon (+338 PgC) is reduced by about half and falls into the range of previous studies (112–323 PgC).

The impact of using the AOGCM result instead of the AOVGCM result is far smaller than the total amount of vegetation, soil, and total carbon storage during the LGM (less than ±50 PgC out of several 1000 PgC; see Table 3) and does not change the main result in the present study. However, these differences are nonnegligible if we try to explain the 100 ppm difference of atmospheric CO_2 concentration between the LGM and the preindustrial era, which corresponds to 200 PgC.

6 Conclusions

In the present study we apply a coupled atmosphere-ocean-vegetation GCM for predicting the LGM climate and vegetation in order to quantify how the vegetation-climate feedback affected the LGM climate. Our sensitivity experiments show tendencies

CPD
8, 5787–5816, 2012

similar to previous paleodata and paleomodeling studies for changes in vegetation and climate. In the present study, vegetation changes during the LGM amplify cooling during the LGM by 13.5 %, which is mostly caused by increases of the land surface albedo. We separate the LGM environment changes into three factors: temperature, precipitation, and CO_2. We then investigate the impact of each of these on the vegetation distribution during the LGM. Separate sensitivity experiments indicate that temperature and precipitation are dominant to the vegetation distribution during the LGM. Low levels of CO_2 during the LGM affects only the tropical regions.

We also investigate terrestrial carbon storage during the LGM by using separate dynamical vegetation modules with GCM variables. The results show that terrestrial carbon storage is generally the same both in pattern and quantity regardless of whether we include vegetation-climate feedback in the input variables. However, the difference is quantitatively comparable to 200 PgC, which corresponds to the CO_2 difference between the LGM (185 ppm) and the preindustrial era (285 ppm). We determine that inclusion of vegetation-climate feedback is nonnegligible if we wish to explain the lowering of atmospheric CO_2 during the LGM.

We separate the terrestrial carbon difference between the LGM and preindustrial era into three factors: response to the LGM climate and CO_2, washout by ice-sheet coverage, and new stock on the exposed continental shelf during the LGM. In the present study, the total reduction of terrestrial carbon (−652 PgC) is explained by −516 PgC due to the LGM environment, −474 PgC removed by the ice sheet, and +338 PgC due to new storage on the exposed continental shelf. The decrease of carbon storage due to the LGM environment is consistent with the previous model and data studies. Washout by the ice sheets depends on how much carbon is stored in these regions in the preindustrial condition. Our results show similar values to those previous studies, regardless of the assumption that carbon is washed out of or stored under the ice. Carbon storage on the exposed continental shelf is larger than that of previous studies because we adopt the largest possible sea-level change, as shown by paleoreconstructions. Carbon

CPD
8, 5787–5816, 2012

storage on the exposed continental shelf falls into the range of variability among previous studies if we assumed the same area as did previous studies.

It is not yet clear where the 200 PgC of carbon is stored; it corresponds to a decrease of 100 ppm of atmospheric CO_2 during the LGM (Lourantou et al., 2010; Ciais et al., 2011; Shakun et al., 2012). When we try to determine the carbon circulation during the LGM, we find that taking vegetation-climate feedback into account is nonnegligible. The difference between total terrestrial carbon storage due to vegetation-climate feedback is comparable to the reduction of atmospheric CO_2, though it is far smaller than total terrestrial carbon storage.

References

Bartlein, P. J., Harrison, S. P., Brewer, S., Connor, S., Davis, B. A. S., Gajewski, K., Guiot, J., Harrison-Prentice, T. I., andO. Peyron, A. H., Prentice, I. C., Scholze, M., Seppa, H., Shuman, B., Sugita, S., Thompson, R. S., Viau, A. E., Williams, J., and Wu, H.: Pollen-based continental climate reconstructions at 6 and 21 ka:a global synthesis, Clim. Dynam., 37, 775–802, 2011. 5789, 5800

Bird, M. I., Lloyd, J. L., and Farquhar, G. D.: Terrestrial carbon storage at the LGM, Nature, 371, 566–566, 1994. 5790

Braconnot, P., Otto-Bliesner, B., Harrison, S., Joussaume, S., Peterchmitt, J.-Y., Abe-Ouchi, A., Crucifix, M., Driesschaert, E., Fichefet, Th., Hewitt, C. D., Kageyama, M., Kitoh, A., Laîné, A., Loutre, M.-F., Marti, O., Merkel, U., Ramstein, G., Valdes, P., Weber, S. L., Yu, Y., and Zhao, Y.: Results of PMIP2 coupled simulations of the Mid-Holocene and Last Glacial Maximum – Part 1: experiments and large-scale features, Clim. Past, 3, 261–277, doi:10.5194/cp-3-261-2007, 2007. 5789, 5799, 5800

Ciais, P., Tagliabue, A., Cuntz, M., Bopp, L., Scholze, M., Hoffmann, G., Lourantou, A., Harrison, S. P., Prentice, I. C., Kelley, D. I., Koven, C., and Piao, S. L.: Large inert carbon pool in the terrestrial biosphere during the Last Glacial Maximum, Nat. Geosci., 5, 74–79, 2011. 5790, 5804

CLIMAP Project Members: The Surface of the Ice-Age Earth, Science, 191, 1131–1137, 1976. 5789

CPD
8, 5787–5816, 2012

CLIMAP Project Members: The Last Interglasial Ocean, Quarternary Res., 21, 123–224, 1984. 5789

Cramer, W., Bondeau, A., Woodward, F. I., Prentice, I. C., Betts, R. A., Brovkin, V., Cox, P. M., Fisher, V., Foley, J. A., Friend, A. D., Kucharik, C., Lomas, M. R., Ramankutty, N., Sitch, S., Smith, B., White, A., and Young-Molling, C.: Global response of terrestrial ecosystem structure and function to CO_2 and climate change: results from six dynamic global vegetation models, Global Change Biol., 7, 357–373, 2001. 5802

Crucifix, M. and Hewitt, C. D.: Impact of vegetation changes on the dynamics of the atmosphere at the Last Glacial Maximum, Clim. Dynam., 25, 447–459, 2005. 5790, 5799

Crucifix, M., Betts, R. A., and Cox, P. M.: Vegetation and climate variability: a GCM modelling study, Clim. Dynam., 24, 457–467, 2005a. 5790, 5800

Crucifix, M., Betts, R. A., and Hewitt, C. D.: Pre-industrial-potential and Last Glacial Maximum global vegetation simulated with a coupled climate-bio sphere model: Diagnosis of bioclimatic relationships, Global Planet. Change, 45, 295–312, 2005b. 5790, 5800

Denman, K. L., Brasseur, G., Chidthaisong, A., Ciais, P., Cox, P. M., Dickinson, R. E., Hauglustaine, D., Heinze, C., Holland, E., Jacob, D., Lohmann, U., Ramachandran, S., daSilbaDias, P. L., Wofsy, S. C., and Zhang, X.: Coupling Between Changes in the Climate System and Biogeochemistry, in: Climate Change 2007 The Physical Science Basis: Contribution of working Groupe I to the Fourth Assesment Report of the Intergovernmental Panel on Climate Change, edited by: Solomon, S., Qin, D., Manning, M., Chen, Z., Marquis, M., Averyt, K. B., Tignor, M., and Miller, H. L., Cambridge university press, Cambridge, 2007. 5802

Faure, H., Adams, J., Debenay, J., Faure-Denard, L., Grants, D., Pirazzoli, P., Thomassin, B., Velichko, A., and Zazo, C.: Carbon storage and continental land surface change since the Last Glacial Maximum, Quarternary Sci. Rev., 15, 843–849, 1996. 5790

François, L. M., Delier, C., Warnant, P., and Munhoven, G.: Modelling the glacial-interglacial changes in the continental biosphere, Global Planet. Change, 17, 37–52, 1998. 5790, 5801

François, L. M., Godderis, Y., Warnant, P., Ramstein, G., de Noble, N., and Lorenz, N.: Carbon stocks and isotopic budgets of the terrestrial biosphere at mid-Holocene and last glacial maximum times, Chem. Geol., 159, 163–189, 1999. 5790, 5801

Friedlingstein, P., Prentice, K. C., Fung, I. Y., John, J. G., and Brasseur, G. P.: Carbon-biosphere-climate interactions in the last glacial maximum climate, J. Geophys. Res., 100, D7203–7221, 1995. 5790, 5801

CPD
8, 5787–5816, 2012

Gerber, S., Joos, F., and Prentice, I. C.: Sensitivity of a dynamic global vegetation model to climate and atmospheric CO_2, Global Change Biol., 10, 1223–1239, 2004. 5790

Harrison, S. P. and Prentice, I. C.: Climate and CO2 controls on global vegetation distribution at the last glacial maximum: analysis based on palaeovegetation data, biome modelling and palaeoclimate simulations, Global Change Biol., 9, 983–1004, 2003. 5789, 5800

Hasumi, H. and Emori, S.: K-1 Coupled GCM (MIROC) Description, k-1 Technical Report No.1, Center for Climate System Research (CCSR, University of Tokyo), National Institute for Environmental Studies (NIES), Frontier Research Center for Global Change (FRCGC), 2004. 5791

Haxeltine, A. and Prentice, I. C.: BIOME3: An equilibrium terrestrial biosphere model based on ecophysiological constraints, resource availability, and competition among plant functional types, Global Biogeochem. Cy., 10, 693–709, 1996. 5792

Henrot, A.-J., François, L., Brewer, S., and Munhoven, G.: Impacts of land surface properties and atmospheric CO_2 on the Last Glacial Maximum climate: a factor separation analysis, Clim. Past, 5, 183–202, doi:10.5194/cp-5-183-2009, 2009. 5790, 5799, 5800

Jahn, A., Claussen, M., Ganopolski, A., and Brovkin, V.: Quantifying the effect of vegetation dynamics on the climate of the Last Glacial Maximum, Clim. Past, 1, 1–7, doi:10.5194/cp-1-1-2005, 2005. 5790, 5800

Joussaume, S. and Taylor, K. E.: The Paleoclimate Modeling Intercomparison Project, WCRP 111: Proceedings of the third PMIP Workshop, 2000. 5789

Jouzel, J., Barkov, N. I., Barnola, J. M., Bender, M., Chappellaz, J., Genthon, C., Kotlyakov, V. M., Lipenkov, V., Lorius, C., Petit, J. R., Raynaud, D., Raisbeck, G., Ritz, C., Sowers, T., Stievenard, M., Yiou, F., and Yiou, P.: Extending the Vostok ice-core record of palaeoclimate to the penultimate glacial period, Nature, 364, 407–412, 1993. 5789, 5790

Kaplan, J. O., Prentice, I. C., Knorr, W., and Valdes, P. J.: Modeling the dynamics of terrestrial carbon storage since the Last Glacial Maximum, Geophys. Res. Lett., 29, 2074, doi:10.1029/2002GL015230, 2002. 5790, 5801

Kohfeld, K. and Harrison, S.: How well can we simulate past climates? Evaluating the models using global palaeoenvironmental datasets, Quaternary Sci. Rev., 19, 321–346, 2000. 5789

Köhler, P. and Fischer, H.: Simulating changes in the terrestrial biosphere during the last glacial/interglacial transition, Global Planet. Change, 43, 33–55, 2004. 5790, 5801

CPD
8, 5787–5816, 2012

Köhler, P., Joos, F., Gerber, S., and Knutti, P.: Simulated changes in vegetation distribution, land carbon storage, and atmospheric CO_2 in response to a collapse of the North Atlantic thermohaline circulation, Clim. Dynam., 25, 689–708, 2005. 5790

Kucera, M., Rosell-Melé, A., Schneider, R., Waelbroeck, C., and Weinelt, M.: Multiproxy approach for the reconstruction of the glacial ocean surface (MARGO), Quaternary Sci. Rev., 25, 813–819, 2005. 5789

Lloyd, J. and Taylor, J. A.: On the temperature-dependent of soil respiration, Funct. Ecol., 8, 315–323, 1994. 5801

Lourantou, A., Lavrič, J. V., Köhler, P., Barnola, J., Paillard, D., Michel, E., Raynaud, D., and Chappellaz, J.: Constrain of the CO_2 rise by new atmospheric carbon isotopic measurements during the last deglaciation, Global Biogeochem. Cy., 24, GB2015, doi:10.1029/2009GB003545, 2010. 5802, 5804

Mahowald, N. M., Muhs, D. R., Levis, S., Rasch, P. J., Yoshioka, M., Zender, C. S., and Luo, C.: Change in atmospheric mineral aerosols in response to climate: Last glacial period, preindustrial, modern, and doubled carbon dioxide climates, J. Geophys. Res., 111, D10202, doi:10.1029/2005JD006653, 2006. 5790

Meehl, G. A., Stocker, T. F., Collins, W. D., Friedlingstein, P., Gaye, A. T., Gregory, J. M., Kitoh, A., Knutti, R., Murphy, J. M., Noda, A., Raper, S. C. B., Watterson, I. G., Weaver, A. J., and Zhao, Z.-C.: Global Climate Projection, in: Climate Change 2007 The Physical Science Basis: Contribution of working Groupe I to the Fourth Assesment Report of the Intergovernmental Panel on Climate Change, edited by: Solomon, S., Qin, D., Manning, M., Chen, Z., Marquis, M., Averyt, K. B., Tignor, M., and Miller, H. L., Cambridge university press, Cambridge, 2007. 5791

Monnin, E., Indermühle, A., Dällenbach, A., Flückiger, J., Stauffer, B., Stocker, T. F., Raynaud, D., and Barnola, J.-M.: Atmospheric CO_2 Concentrations over the Last Glacial Termination, Science, 291, 112–114, 2001. 5789, 5790

Montenegro, A., Eby, M., Kaplan, J. O., Meissner, K. J., and Weaver, A. J.: Carbon storage on exposed continental shelves during the glacial-interglacial transition, Geophys. Res. Lett., 33, L08703, doi:10.1029/2005GL025480, 2006. 5790, 5802

O'ishi, R. and Abe-Ouchi, A.: Influence of dynamic vegetation on climate change arising from increasing CO_2, Clim. Dynam., 33, 645–663, 2009. 5791, 5792

CPD
8, 5787–5816, 2012

O'ishi, R. and Abe-Ouchi, A.: Polar amplification in the mid-Holocene derived from dynamical vegetation change with a GCM, Geophys. Res. Lett., 38, L14702, doi:10.1029/2011GL048001, 2011. 5791, 5792
Otto, D., Rasse, D., Kaplan, J. O., Warnant, P., and François, L.: Biospheric carbon stocks reconstructed at the Last Glacial Maximum: comparison between general circulation models using prescribed and computed sea surface temperatures, Global Planet. Change, 33, 117–138, 2002. 5790, 5801
Peltier, W. R.: Ice Age Paleotopography, Science, 265, 195–201, 1994. 5789
Peltier, W. R.: Global glacial isostasy and the surface of the ice-age earth: The ice-5G (VM2) model and grace, Annu. Rev. Earth Pl. Sc., 32, 111–149, 2004. 5789, 5793
Prentice, I. C. and Harrison, S. P.: Ecosystem effects of CO_2 concentration: evidence from past climates, Clim. Past, 5, 297–307, doi:10.5194/cp-5-297-2009, 2009. 5789, 5790
Prentice, I. C. and Jolly, D.: Mid-Holocene and glacial-maximum vegetation geography of the northern continents and Africa, J. Biogeogr., 27, 507–519, 2000. 5789, 5800
Prentice, I. C. and Webb, T.: BIOME 6000: reconstructing global mid-Holocene vegetation patterns from palaeoecological records, J. Biogeogr., 25, 997–1005, 1998. 5789
Prentice, I. C., Sykes, M. T., Lautenschlager, M., Harrison, S. P., Denissenko, O., and Bartlein, P. J.: Modelling global vegetation patterns and terrestrial carbon storage at the last glacial-maximum, Global Ecol. Biogeogr. Lett., 3, 67–76, 1993. 5790, 5801
Prentice, I. C., Harrison, S. P., and Bertlein, P. J.: Global vegetation and terrestrial carbon cycle changes after the last ice age, New Phytol., 189, 988–998, 2011. 5789, 5800
Shakun, J. D., Clark, P. U., He, F., Marcott, S. A., Mix, A. C., Liu, Z., Otto-Bliesner, B., Schmittner, A., and Bard, E.: Global warming preceded by increasing carbon dioxide concentrations during the last deglaciation, Nature, 484, 49–54, 2012. 5804
Sitch, S., Smith, B., Prentice, I. C., Arneth, A., Bondeau, A., Cramer, W., Kaplan, J. O., Levis, S., Lucht, W., Sykes, M. T., Thonicke, K., and Venevsky, S.: Evaluation of ecosystem dynamics, plant geography and terrestrial carbon cycling in the LPJ dynamic global vegetation model, Global Change Biol., 9, 161–185, 2003. 5791, 5802
Takata, K., Emori, S., and Watanabe, T.: Development of the minimal advanced treatments of surface interaction and runoff, Global Planet. Change, 38, 209–222, 2003. 5792
Takemura, T., Egashira, M., Matsuzawa, K., Ichijo, H., O'ishi, R., and Abe-Ouchi, A.: A simulation of the global distribution and radiative forcing of soil dust aerosols at the Last Glacial Maximum, Atmos. Chem. Phys., 9, 3061–3073, doi:10.5194/acp-9-3061-2009, 2009. 5790

CPD
8, 5787–5816, 2012

Uppala, S. M., Kallberg, P. W., Simmons, A. J., da Costa Bechtold, U. A. V., Fiorino, M., Gibson, J. K., Haseler, J., Hernandez, A., Kelly, G. A., Li, X., Onogi, K., Saarinen, S., Sokka, N., Allan, R. P., Andersson, E., Arpe, K., Balmaseda, M. A., Beljaars, A. C. M., van de Berg, L., Bidlot, J., Bormann, N., Caires, S., Chevallier, F., Dethof, A., Dragosavac, M., Fisher, M., Fuentes, M., Hagemann, S., Hólm, E., Hoskins, B. J., Isaksen, L., Janssen, P. A. E. M., Jenne, R., McNally, A. P., Mahfouf, J. F., J, J. M., Rayner, N. A., Saunders, R. W., Simon, P., Sterl, A., Trenberth, K. E., Untch, A., Vasiljevic, D., Viterbo, P., and Woollen, J.: The ERA-40 re-analysis, Q. J. Roy. Meteorol. Soc., 131, 2961–3012, doi:10.1256/qj.04.176, 2005. 5792

Wyputta, U. and McAvaney, B. J.: Influence of vegetation changes during the Last Glacial Maximum using the BMRC atmospheric general circulation model, Clim. Dynam., 17, 923–932, 2001. 5790

Xie, P. and Arkin, P. A.: A 17-year monthly analysis based on gauge observations, satellite estimates, and numerical model outputs, B. Am. Meteorol. Soc., 78, 2539–2558, 1997. 5792

Yokoyama, Y., Lambeck, K., DeDeckker, P., Johnston, P., and Fifield, L. K.: Timing of the Last Glacial Maximum from observed sea-levelminima, Nature, 406, 713–716, 2000. 5789, 5802

Yu, G., Chen, X., Ni, J., Cheddadi, R., Guiot, J., Han, H., Harrison, S. P., Huang, C., Ke, M., Kong, Z., Li, S., Li, W., Liew, P., Liu, G., Liu, J., Liu, Q., Liu, K.-B., Prentice, I. C., Qui, W., Ren, G., Song, C., Sugita, S., Sun, X., Tang, L., Campo, E. V., Xia, Y., Xu, Q., Yan, S., Yang, X., Zhao, J., and Zheng, Z.: Palaeovegetation of China: a pollen data-based synthesis for the mid-Holocene and last glacial maximum, Journal of Biogeography, 27, 635–664, 2000. 5789

Zeng, N.: Glacial-Interglacial Atmospheric CO_2 Change The Glacial Burial Hypothesis, Adv. Atmos. Sci., 20, 677–693, 2003. 5790, 5802

Zeng, N.: Quasi-100 ky glacial-interglacial cycles triggered by subglacial burial carbon release, Clim. Past, 3, 135–153, doi:10.5194/cp-3-135-2007, 2007. 5802

CPD
8, 5787–5816, 2012

Table 1. Settings of the experiments performed in this study.

Experiment	CO_2 level	Orbit	Vegetation	MIROC-LPJ	separated LPJ-DGVM
AOV (PI)	285 ppm	0 ka	dynamic	390 yr	1000 yr
AOV (LGM)	185 ppm	LGM	dynamic	400 yr	1000 yr
AO (PI)	285 ppm	0 ka	fixed to AOV (PI)	75 yr	–
AO (LGM)	185 ppm	LGM	fixed to AOV (PI)	50 yr	1000 yr

CPD
8, 5787–5816, 2012

Table 2. Settings of the sensitivity experiments performed in this study. Precipitation and temperature are taken from the AOV (LGM) and the AOV (PI), respectively.

Experiment	CO_2	Precipitation	Temperature
CP	185 ppm	LGM	PI
TC	185 ppm	PI	LGM
TP	285 ppm	LGM	LGM

CPD
8, 5787–5816, 2012

Table 3. Equilibrium carbon storage (PgC). Values in the parentheses do not include the LGM ice-sheet area in the PI or continental shelf area in the LGM.

Experiment	Vegetation	Soil	Total
AOV (PI)	1094.9 (985.2)	1727.3 (1363.1)	2822.2 (2348.3)
AO (LGM)	825.7 (662.4)	1313.9 (1120.6)	2139.6 (1783.0)
AOV (LGM)	830.3 (671.6)	1340.6 (1160.8)	2170.9 (1832.4)

CPD
8, 5787–5816, 2012

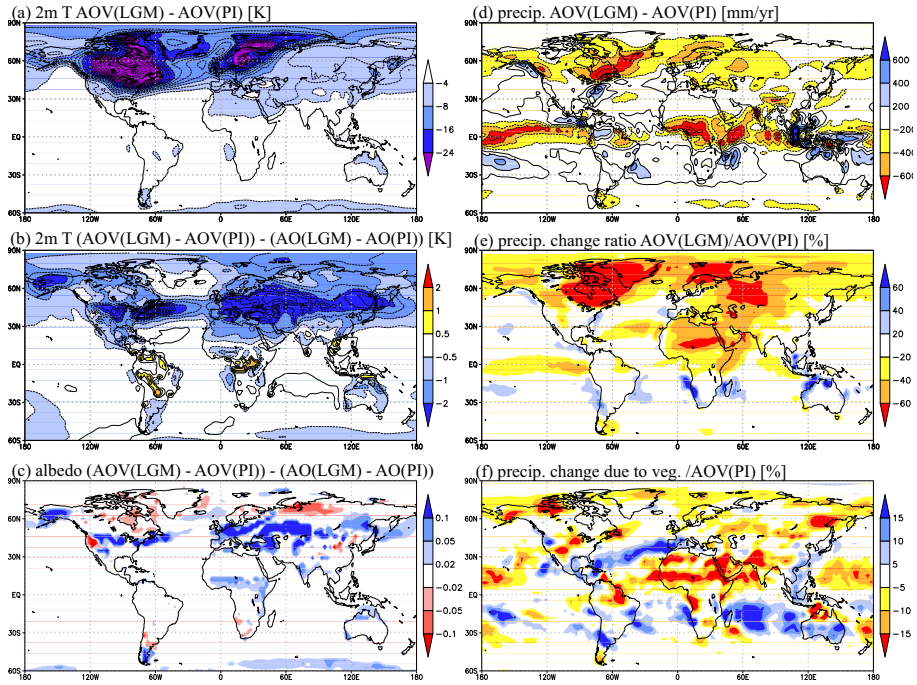

Fig. 1. Annual averaged **(a)** cooling [K] in the experiment AOV (LGM) (the contour interval is 2 K), **(b)** contribution of DGVM to this cooling [K] in the AOV (LGM), which was calculated as (AOV (LGM) – AOV (PI)) – (AO (LGM) – AO (PI)) (the contour interval is 1 K), **(c)** contribution of the DGVM to the change in surface albedo, **(d)** precipitation change [mm yr^{-1}] in the experiment AOV (LGM) (the contour interval is 100 mm yr^{-1}), **(e)** precipitation change ratio [%] in the LGM compared to the PI, and **(f)** contribution of vegetation change to the precipitation change in the LGM compared to the PI.

CPD
8, 5787–5816, 2012

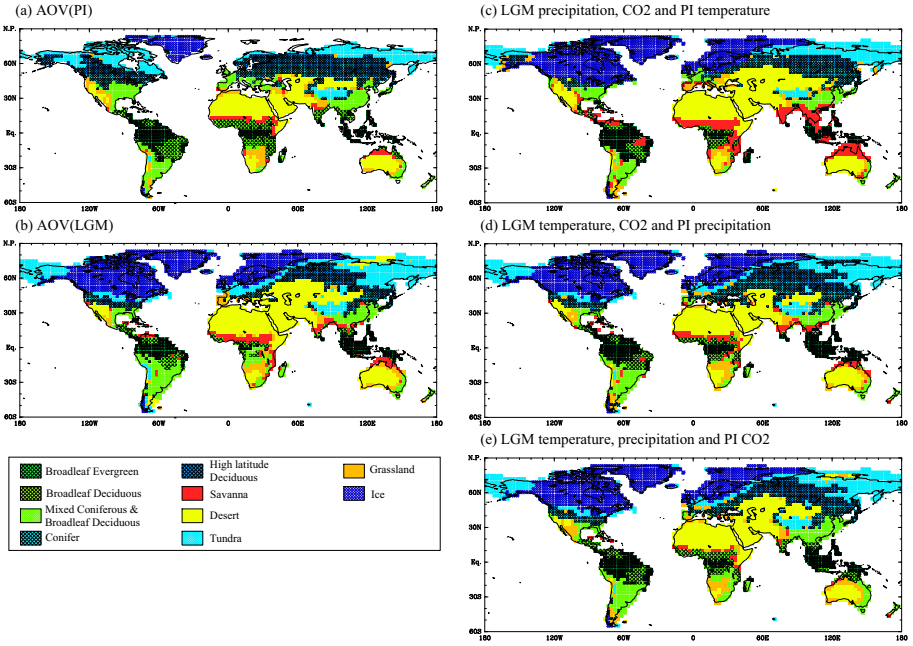

Fig. 2. Potential vegetation distribution obtained in **(a)** preindustrial, **(b)** LGM, **(c)** sensitivity exp. CP, **(d)** sensitivity exp. TC, and **(e)** sensitivity exp. TP.

CPD
8, 5787–5816, 2012

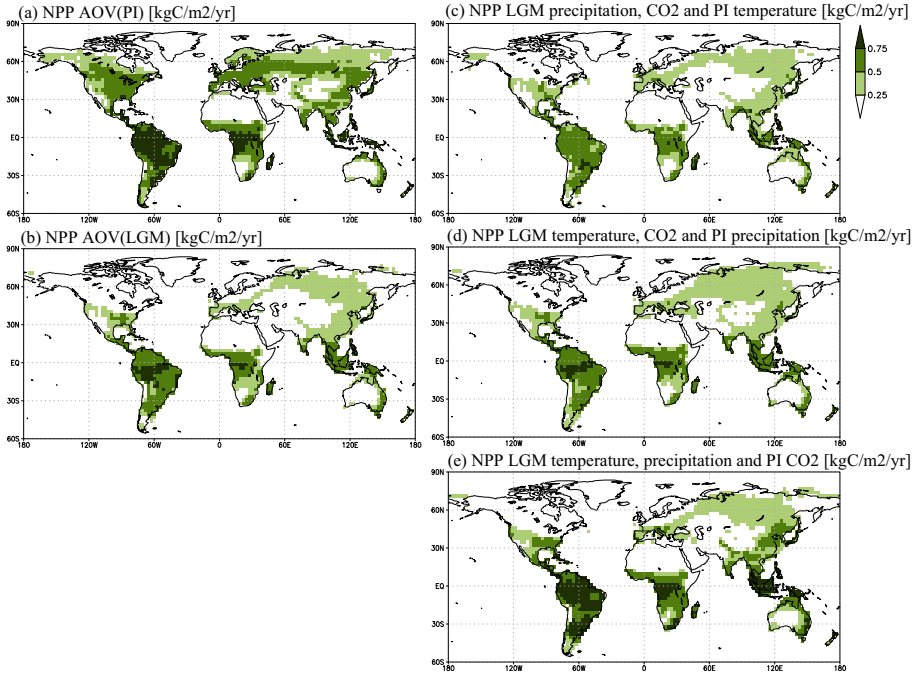

Fig. 3. Annual NPP [kgC m^{-2} yr^{-1}] distribution obtained for **(a)** preindustrial era, **(b)** LGM, **(c)** sensitivity exp. CP, **(d)** sensitivity exp. TC, and **(e)** sensitivity exp. TP.

CPD
8, 5787–5816, 2012

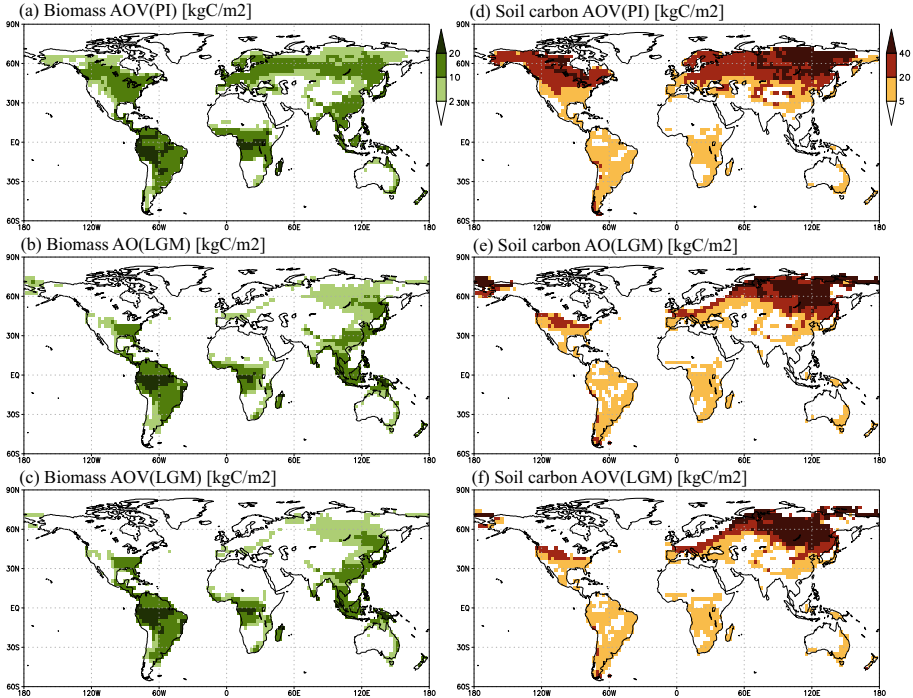

Fig. 4. Equilibrium vegetation carbon [kgC m^{-2}] obtained from **(a)** AOV (PI), **(b)** AO (LGM), and **(c)** AOV (LGM); and equilibrium litter and soil carbon obtained from **(d)** AOV (PI), **(e)** AO (LGM), and **(f)** AOV (LGM).

CPD
8, 5787–5816, 2012